RSC Advances

PAPER

View Article Online
View Journal | View Issue



Cite this: *RSC Adv.*, 2017, **7**, 46155

# Is nano $ZrO_2$ a better photocatalyst than nano $TiO_2$ for degradation of plastics?

W. R. L. Nisansala Bandara,[ab] Rohini M. de Silva,*[a] K. M. Nalin de Silva,[ab] Damayanthi Dahanayake,[b] Sunanda Gunasekara[b] and Kulatheepan Thanabalasingam[b]

The environmental accumulation of plastic is a huge problem due to its low degradability. There are solutions to this problem such as reusing, recycling and the use of biodegradable plastics. However, a complete solution to this problem has not yet been achieved. In this study, photocatalytic degradation of polyethylene and polyropylene was investigated. The effect of $ZrO_2$ nanoparticles in comparison with $TiO_2$ nanoparticles for photocatalytic degradation was studied. $TiO_2$ nanoparticles were synthesized by a sol gel method and $ZrO_2$ nanoparticles were synthesized by a sonochemical method. The $TiO_2$ and $ZrO_2$ particles were characterized using FTIR, XRD, UV visible spectroscopy, EDX, SEM, and TEM. Both types of particles were approximately 50 nm in size. $TiO_2$ nanoparticles were tetragonal and in the anatase phase. $ZrO_2$ particles were tetragonal and nano porous. The application of these particles to polyethylene and polypropylene was performed using nanoparticle suspensions in a THF medium. The degradation of the plastics was studied by investigating chemical changes using FTIR and morphological changes using SEM. Optimization of the concentration and exposure time was performed under laboratory conditions using a sun simulator. Polyethylene and polypropylene were treated under the sun simulator as well as under the real sun light conditions. In both treatment conditions, it was found that there is a significant difference in the degradation of plastics and $ZrO_2$ nanoparticle suspension treated polyethylene and polypropylene showed higher degradation than the $TiO_2$ nanoparticle suspension treated samples at 95% confidence levels.

Received 27th July 2017
Accepted 25th September 2017

DOI: 10.1039/c7ra08324f

rsc.li/rsc-advances



## 1. Introduction

Plastics, including polyolefins, are manmade long chain polymer molecules, which are widely used in manufacturing kitchen appliances, furniture, toys, *etc.* With the increasing demand for plastic products, these materials are being synthesized on a large scale. In addition, properties such as light weight, hydrophobicity, transparency, chemical resistance, durability, flexibility, and ease of cleaning have made these materials attractive for various applications. Currently plastics have become the most widely manufactured materials in the world due to these properties.

Basic raw materials for the synthesis of plastics come from extractions from oil, coal and natural gases. Plastics have been categorized into different types such as polyethylene (PE), polypropylene (PP), polystyrene (PS), polyvinylchloride (PVC), polyurethane (PU), polyethylene terephthalate (PET), polybutylene terephthalate (PBT) and nylons, depending on the monomer unit present in the polymer.[1]

Plastics have poor biodegradability and their waste persists in the environment for many years. This leads to a major environmental threat in many parts of the world.[2] Accumulated plastic waste may have adverse health effects, and minimizes the efficient use of land. Plastic pollution in the terrestrial and the marine environment presents a direct threat to wildlife and marine life.

Land filling has been a traditional solution to plastic waste management.[3] However, this has been identified as a temporarily solution, because of the increasing rate of plastic waste accumulation. Therefore attention has been given to recycling, reusing and reducing the use of plastics. Although these kinds of steps have been taken as solutions to the plastic waste problem, they do not adequately address the ever growing amount of plastic waste originating from households. As a result, bio-degradable plastics were developed.[4] Nevertheless plastic pollution is still a great threat to the environment. Photocatalytic degradation of plastic can be a viable option. This is a low temperature process with economic advantages.[5]

$TiO_2$ is an inorganic oxide which exists in three different phases, namely, anatase, rutile, and brookite. Anatase and rutile are the active crystalline phases of $TiO_2$.[6] $TiO_2$ has a band gap varying from 3.0 eV to 3.2 eV (ref. 7) and it is a nontoxic semiconductor. Because of the high photo catalytic activity of $TiO_2$, it

[a]*Department of Chemistry, Faculty of Science, University of Colombo, Colombo 03, Sri Lanka. E-mail: rohini@chem.cmb.ac.lk*

[b]*Sri Lanka Institute of Nanotechnology (SLINTEC), Nanotechnology and Science Park, Mahenwatta, Pitipana, Homagama, Sri Lanka*

has been used for various applications such as for water and air purification,[8] degradation of organic compounds,[9] dye sensitized solar cells,[10] sterilization,[11] disinfection,[12] self-cleaning[13] fabrics, and photo induced water splitting.[14] The photo catalytic activity of $TiO_2$ depends on the crystalline structure, crystalline size and the morphology. Due to characteristics such as inexpensiveness, good photo stability, non-toxicity and high reactivity, $TiO_2$ has been generally regarded as a good photocatalyst.[15]

$ZrO_2$ is a transition metal oxide which is nontoxic, chemically inert and thermally stable. Pure $ZrO_2$ exists in three crystallographic phases namely monoclinic, tetragonal and cubic.[16] $ZrO_2$, has a wide band gap. The band gap energy of nano $ZrO_2$ particles varies from 3.3 eV to 5.1 eV.[17] Zirconia has useful chemical and physical properties such as high thermal and chemical stability, low thermal conductivity, high corrosion resistance, high strength and fracture toughness. Hence zirconia is used in oxygen sensors,[18] fuel cells,[19] catalyst and catalytic supports,[20–23] high dielectric material[24] for large scale integrated circuits and as gate dielectric in metal oxide semiconductors.

Currently nanomaterials have been identified as potential catalysts to degrade plastics with enhanced properties. Metal oxide nanoparticles have been blended with the plastics in order to enhance the degradation by the photo catalytic effect. Use of $TiO_2$ in degradation of plastics is well known. However, use of pure $ZrO_2$ has not been recorded before. This study is focused on the investigation of the catalytic ability of $ZrO_2$ as compared to $TiO_2$, towards the degradation of polyethylene and polypropylene.

## 2. Experimental section

### 2.1 Materials

Polyethylene (gauge size 80) and polypropylene (gauge size 200) samples were purchased from the local market, Sri Lanka. Titanium tetraisopropoxide (TTIP, 97%), zirconium nitrate (99%), potassium iodide (99%), phthalic acid (99.5%), tetrahydrofuran (THF, 99.9%), methanol (99.9%), ethanol (99.8%), and nitric acid (70%) were all analytical grade and purchased from Sigma Aldrich.

### 2.2 Synthesis of $TiO_2$ nanoparticles

A volume of 5 ml TTIP (molecular weight 283.8 g $mol^{-1}$) was dissolved in 15 ml of isopropanol and stirred for 1 hour at 1000 rpm at room temperature. A solution of nitric acid at pH 2 (250 ml) was prepared using deionized water and $HNO_3$. The acid solution was added drop wise to the mixture while stirring. The white slurry was aged for 48 hours. This suspension was centrifuged at 9000 rpm for 30 minutes. The resulting precipitate was washed twice with ethanol. The resulting precipitate was heated for 2 hours at 100 °C. Then the solid was heated at 450 °C for 1 hour.[6]

### 2.3 Synthesis of $ZrO_2$ nanoparticles

$Zr(NO_3)_4 \cdot 3H_2O$ (10.17 g, 30 mmol) and KI (5.1 g, 30 mmol) were mixed with 30 ml of methanol. Isophthalic acid (5.1 g, 10 mmol) was also dissolved in 30 ml of methanol. Both solutions were sonicated separately for 30 minutes. Then the two solutions were mixed together and sonicated for further 30 minutes. The mixture was centrifuged for 15 minutes at 400 rpm. The resulting yellow precipitate was washed twice with deionized water. Then it was washed with acetone. The precipitate was decomposed at 220 °C for 1 hour. Then it was heated at 700 °C for 4 hours in the muffle furnace.[25]

### 2.4 Preparation of nanoparticle dispersion

The $TiO_2$ and $ZrO_2$ nanoparticle solutions were prepared to following concentrations: 6000 ppm, 7000 ppm, 8000 ppm, 9000 ppm, 10 000 ppm, 11 000 ppm and 20 000 ppm. This was done by dispersing 6, 7, 8, 9, 10, 11, and 20 mg of nanoparticles, respectively, in 1.0 ml of THF, and sonicating for 30 min.

### 2.5 Application of the dispersion of nanoparticles to polyethylene and polypropylene samples

Polyethylene and polypropylene samples were cut into 1.5 cm × 1.5 cm squares. A volume of 200 μL of each dispersion of nanoparticles was spread on a plastic square. The nanoparticle suspensions with concentrations of 6000 ppm, 7000 ppm, 8000 ppm, 9000 ppm, 10 000 ppm, 11 000 ppm and 20 000 ppm were used to find the optimize concentration. After the evaporation of the tetrahydrofuran, the treated samples were kept under the sun simulator and under the real sunlight. The samples were kept for 20 hours, 40 hours, 60 hours, 80 hours and 100 hours under the sun simulator for time optimization. One hour under the sun simulator is equivalent to 10 hours under the real sunlight. The samples were treated under the real sunlight, 4 hours per day (9 am to 1 pm) for consecutive days until it completes 20 hours and 100 hours. The applied nanoparticle coating was washed by the tap water before taking the FTIR measurements.

### 2.6 Determination of plastic degradation

The qualitative and quantitative detection of the carbonyl group which appears as the degradation of polymer was done by the absorption mode of FTIR studies on each treated plastic sample using FTIR in ATR-IR mode. For each sample, a number of 64 scans with resolution 4 $cm^{-1}$ were recorded in absorbance units from 4000 $cm^{-1}$ to 600 $cm^{-1}$. The Carbonyl Index (CI) of each plastic sample was calculated. The morphological studies of the polymer surface was done by obtaining SEM images of the samples.

### 2.7 Characterization

The sizes and morphologies of the synthesized $TiO_2$ and $ZrO_2$ nanoparticles were analyzed using a Hitachi SU6600 Scanning Electron Microscope with EDX system (Thermo Scientific) and JEOL JEM-2100 Transmission Electron Microscope at 200 kV.

The phase purity of the products was verified by a Bruker D8 PXRD using Cu $K\alpha^{-1}$ radiation.

Bruker FTIR spectrometer of the vertex series was used to characterize the nanoparticles including the determination of degradation of plastic using absorption spectrum. Sixty-four

 

scans of symmetrical interferograms were averaged and the spectrum was calculated from 4000 to 600 $cm^{-1}$ at a spectral resolution of 4 $cm^{-1}$. For the integration measurements of the carbonyl peak and the $CH_2$ peak OPUS version 6.0 software was used.

US 900 Sun simulator was used to simulate the sun light.

A Shimadzu UV visible spectrophotometer was used for the determination of the band gap energy of the prepared nanoparticles.

# 3. Results and discussion

## 3.1 Characterization of $TiO_2$ and $ZrO_2$ nanoparticles

In the FTIR spectrum of $TiO_2$ the band centred around 3400 $cm^{-1}$ and 1650 $cm^{-1}$ in Fig. 1(a) are due to the stretching and bending vibrations of hydroxyl groups. The peak around 3400 $cm^{-1}$ is ascribed to the hydroxyl group of Ti–OH. The weak peak around 1650 $cm^{-1}$ is associated with the deformation vibration of H–O–H bonds which results due to the fact the spectra were recorded *in situ* and re-desorption of water from the atmosphere is possible.[26–28] The peak centred around 550 $cm^{-1}$ is due to the stretching vibration of Ti–O bond. The peaks around 1450 $cm^{-1}$ are a result of Ti–O–Ti stretching vibrations.[6] This is in good agreement with the published data.

In the FTIR spectra of $ZrO_2$ the broad peak around 3400 $cm^{-1}$ and the sharp peaks around 1650 $cm^{-1}$ in Fig. 1(b) are due to the stretching and bending vibrations of the hydroxyl groups resulting from the absorption of the water molecules. The band around 1400 $cm^{-1}$ is due to the adsorption of non-bridging OH groups.[29,30] The peaks around 540 $cm^{-1}$ and 700 $cm^{-1}$ arise from the Zr–O vibrations of the tetragonal $ZrO_2$.[29,31] A sharp band around 750 $cm^{-1}$ is characteristic for monoclinic $ZrO_2$.[30] Interestingly, a peak near 750 $cm^{-1}$ cannot be seen in this spectrum. Therefore, it can be presumed that monoclinic $ZrO_2$ is not present in the sample.

The X-ray diffractogram of a nano $TiO_2$ sample in Fig. 2(a) exhibits the pattern that is similar to anatase $TiO_2$. All the peaks are in good agreement with JCPDS #89-4921. The XRD pattern of the prepared sample showed peaks at 25.1°, 37.7°, 47.7°, and 53.8° corresponding to the tetragonal anatase crystal planes of (101), (004), (200) and (105) respectively.[6,14] It is noted that the XRD peaks of nano $TiO_2$ are broader than those of bulk $TiO_2$ as expected, due to the smaller crystalline size compared to the bulk.[32] The average crystallite size of the tetragonal phase of anatase $TiO_2$ calculated from the (101) diffraction peak was found to be 8.20 nm. The *d* spacing value for the prominent peak of the 101 plane is 0.35 nm.

The X-ray diffractogram of a prepared $ZrO_2$ sample in Fig. 2(b) is phase pure, agreeing well with JCPDS #80-0965. High diffraction peaks at 30.1°, 35.1°, 50.2° and 60.4° correspond to the (101), (110), (112) and (211) planes, and low intensity peaks at 33.6°, 50.8°, and 59.3° correspond to the (002), (200), and (103) tetragonal phase of $ZrO_2$ respectively. However, the assignment of cubic and tetragonal structures based solely on the X-ray diffraction analysis can be misleading as the diffraction peaks of cubic phase coincide with the major peaks in the tetragonal phase.[33] It can be verified that the prepared sample contains tetragonal phase with the presence of characteristic splitting of

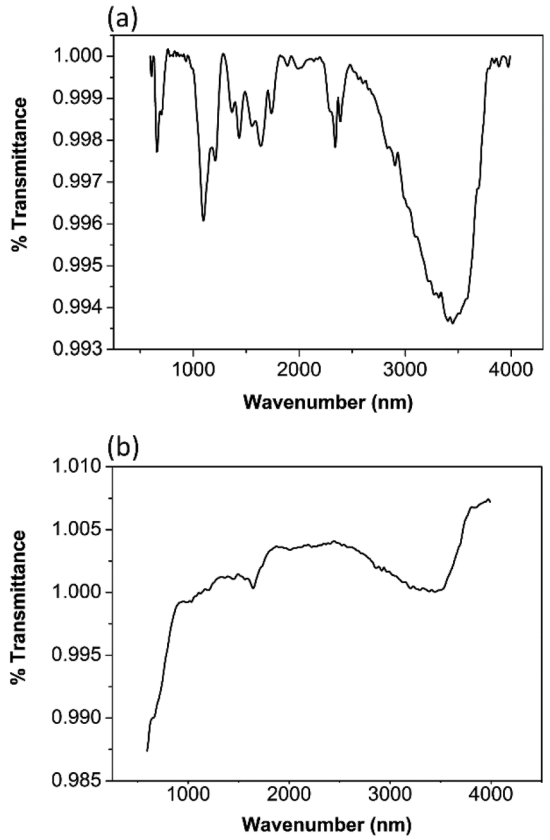


Fig. 1 FTIR of (a) $TiO_2$ (b) $ZrO_2$.

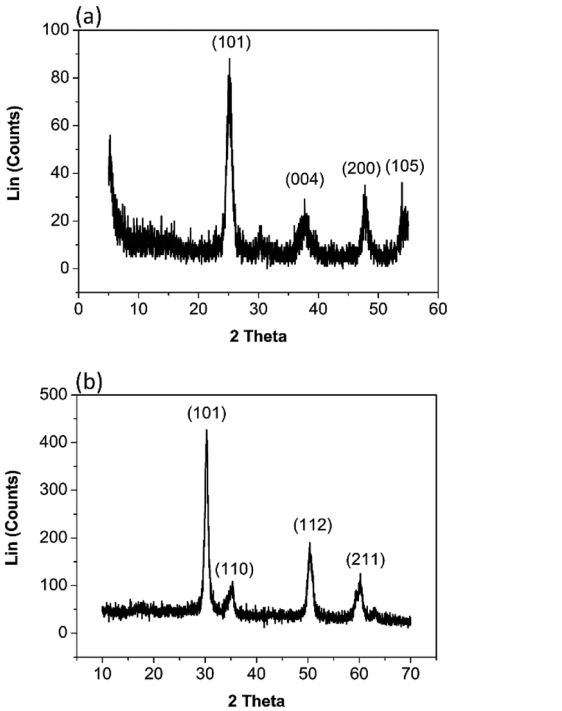


Fig. 2 XRD of (a) $TiO_2$ (b) $ZrO_2$.

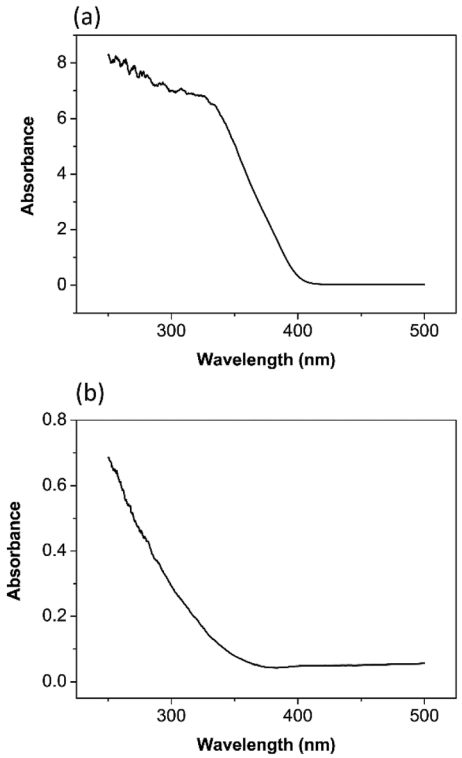


Fig. 3 UV/vis spectroscopy of (a) $TiO_2$ (b) $ZrO_2$.

the diffraction peaks, whereas the cubic phase exhibits only single peaks. Thus our $ZrO_2$ sample has a tetragonal phase or it might be a mixture of tetragonal phase and cubic phase.[33] The average crystallite size of the prepared $ZrO_2$ calculated from (101) diffraction peak was estimated as 10.97 nm. The *d* spacing value of the prominent (101) plane is 0.29 nm.

According to the UV visible spectrum of $TiO_2$ nanoparticles in Fig. 3(a), it has an absorbance due to band gap transition at 413 nm. The band gap energy was calculated as 3.0 eV.[34] It is reported in the literature that the anatase phase has a band gap of 3.2 eV.[7,35]

The UV visible spectrum of $ZrO_2$ nanoparticles in Fig. 3(b) has an absorbance due to band gap transition at 365 nm. The band gap energy was calculated as 3.4 eV.[36] Basahel[33] estimated the band gap energy for monoclinic $ZrO_2$ as 3.25 eV, tetragonal $ZrO_2$ as 3.58 eV, and cubic $ZrO_2$ as 4.33 eV. Comparison with this literature data provides evidence that the tetragonal phase of $ZrO_2$, rather than the cubic, has been synthesized by the procedure described above.

According to the SEM micrograph of the prepared $TiO_2$ nanoparticles in Fig. 4(a) and $ZrO_2$ nanoparticles in Fig. 4(c) it can be confirmed that the particle size is less than 100 nm. Heavy agglomeration was observed in both particles, which may be due to the calcination process, as previously observed.[37]

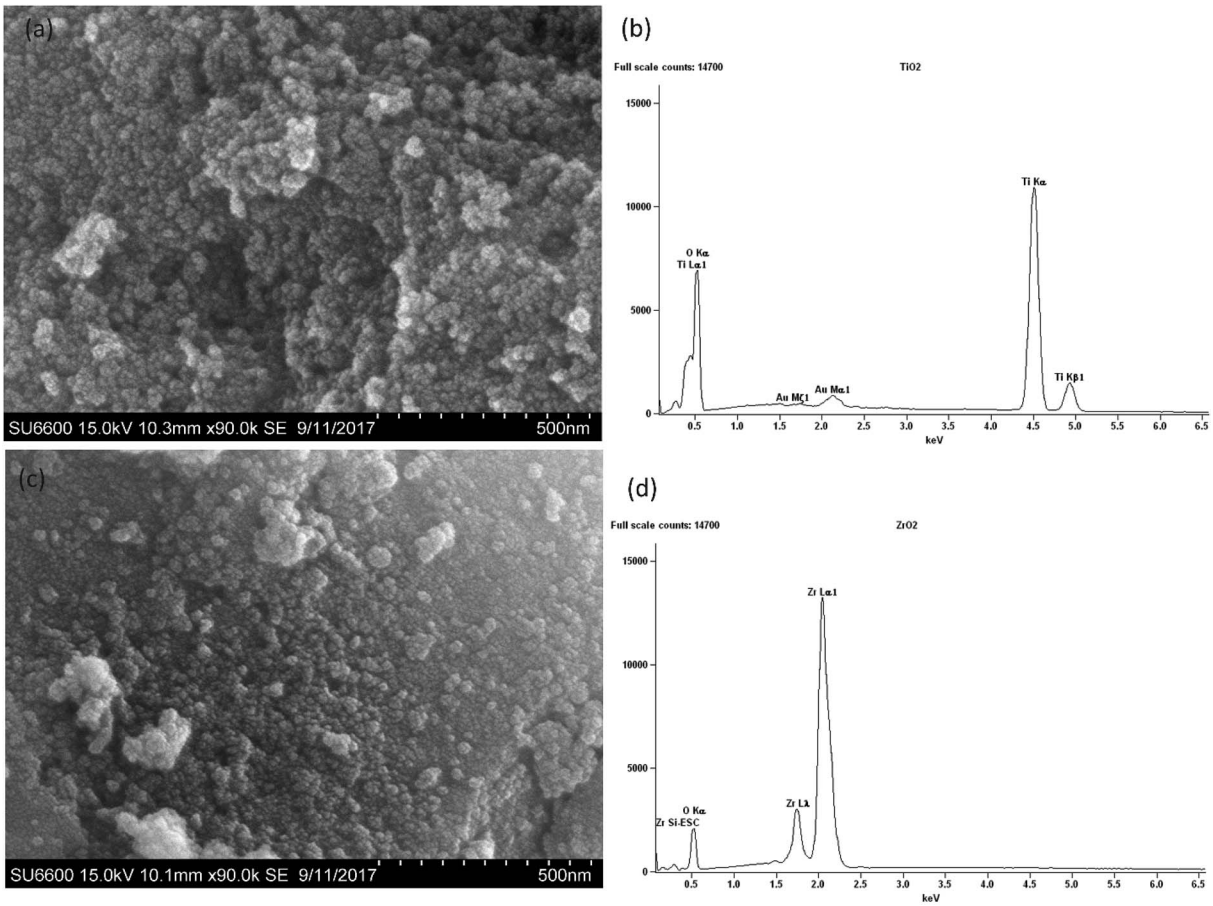


Fig. 4 SEM images of nano (a) $TiO_2$ (c) $ZrO_2$, EDX analysis of (b) $TiO_2$ (d) $ZrO_2$.

 

However it can be observed that the majority of $TiO_2$ particles and $ZrO_2$ particles are around 50 nm in size.

The EDX spectra of the prepared nanoparticles show the elemental composition of the sample. The spectrum of $TiO_2$ in Fig. 4(b) confirms the presence of Ti and O,[38] while the spectrum of $ZrO_2$ in Fig. 4(d) confirms the presence of Zr and O.[38]

According to the TEM images shown in Fig. 5(a) and (b) both $TiO_2$ and $ZrO_2$ particle shapes are irregular and agglomerations

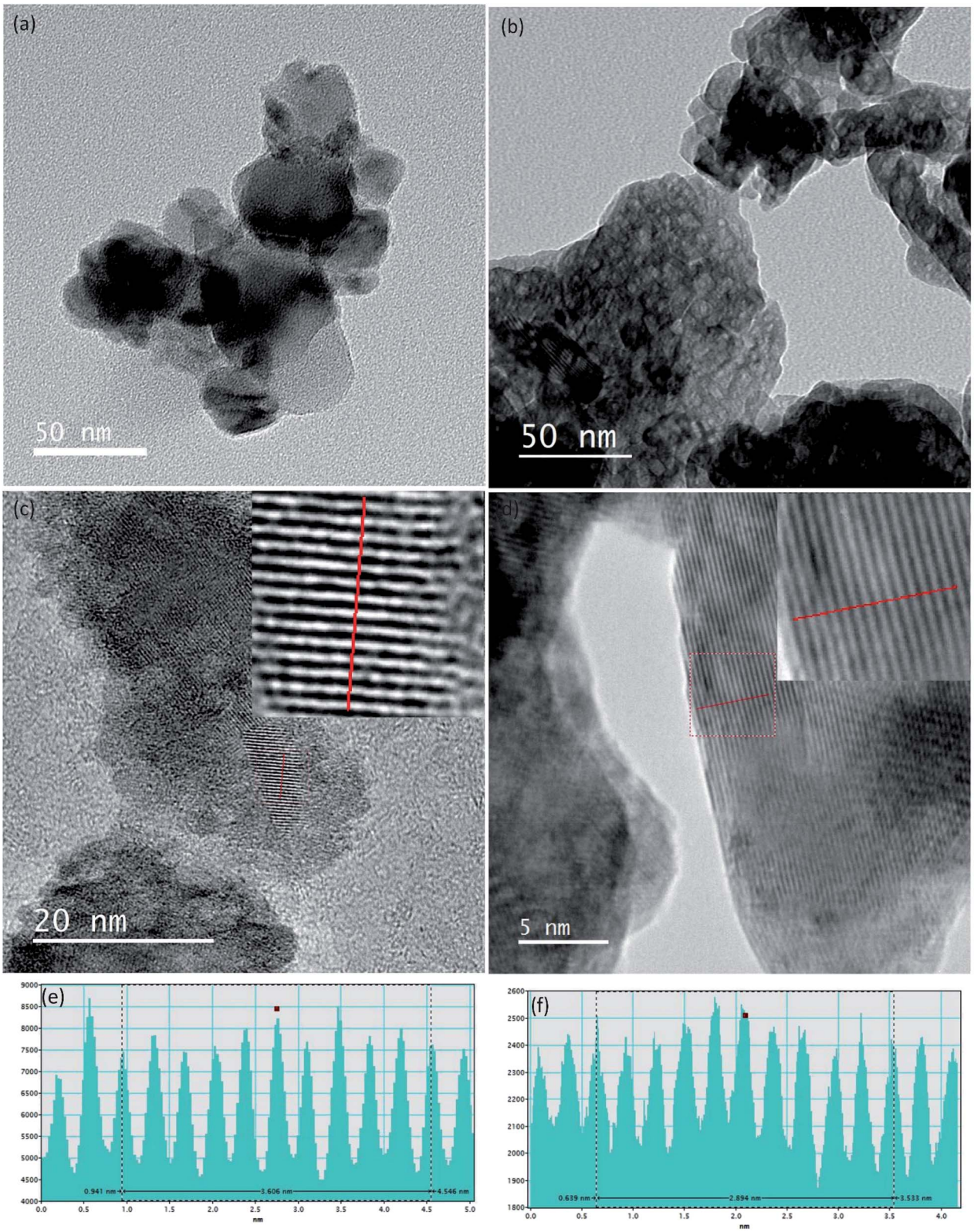


Fig. 5 TEM images of nano (a) $TiO_2$ (b) $ZrO_2$, HRTEM image of nano (c) $TiO_2$ (d) $ZrO_2$, line profile of the HRTEM image (e) $TiO_2$ (f) $ZrO_2$.

are clearly visible. The particle sizes of $TiO_2$ and $ZrO_2$ vary from 15 nm to 55 nm and 5 nm to 60 nm respectively. High resolution TEM image of $TiO_2$ and $ZrO_2$ nanoparticles are given in the Fig. 5(c) and (d) which clearly show the well resolved equidistant lattice fringes. The atomic interlayer distance of $TiO_2$ was calculated to be 0.36 nm (Fig. 5(e)) which can be attributed to the interplanar spacing corresponding to the 101 plane of the anatase phase of $TiO_2$. The atomic interlayer distance of $ZrO_2$ was calculated to be 0.29 nm (Fig. 5(f)) which can be attributed to the interplanar spacing corresponding to the 101 plane of the tetragonal phase of $ZrO_2$. It can be clearly seen in Fig. 5(b) that $ZrO_2$ has a nanoporous structure and the average pore size varies from 3 nm to 10 nm.

### 3.2 Degradation of polyethylene (PE) and polypropylene (PP)

The degradation of PE and PP was determined by morphological studies and statistical studies. The morphology of the PE and PP was studied using SEM images. The carbonyl index was calculated using FTIR data.

**3.2.1 Morphological studies of degradation of plastic.** The morphological studies of degradation of PE shows that, with the increasing $ZrO_2$ concentration on the PE film, the damage to the PE surface has increased, in Fig. 6(b–f) with respect to the pure PE film (Fig. 6(a)). The surface of the PE sample treated with 10 000 ppm $TiO_2$ suspension and kept under the sun simulator for 100 hours (Fig. 6(h)) showed more degradation than the surface of the PE sample in Fig. 6(g) which kept under the same light source for 20 hours. Thus the damage to the PE surface increases with increased exposure to the light source.

The SEM image of PP film in Fig. 7(c), which was treated with 10 000 ppm $ZrO_2$ suspension and kept under real sun light for 20 hours, shows more damage than the PP film in Fig. 7(b) which was treated with 10 000 ppm $TiO_2$ suspension and kept under the same conditions. Likewise, the SEM image of PE film in Fig. 7(e) which was treated with 10 000 ppm $ZrO_2$ suspension and kept under real sun light for 20 hours shows more damage than the PE film in Fig. 7(d) which was treated with 10 000 ppm $TiO_2$ suspension and kept under the same conditions.

**3.2.2 Statistical studies of degradation of plastic.** Attenuated Total Reflectance (ATR) is a mid IR spectroscopic technique which is one of the most important spectroscopic methods that can be used for the identification and quantification of the oxidation process of a polymer material.[39] ATR/FTIR spectroscopy is commonly performed at a single point on the sample surface that is determined to be representative of the sample to be examined.[40] This technique penetrates a thin layer of a sample and measures the carbonyl formation on the surface of the material.[39]

In order to determine the best nanoparticle concentration for the given mass of PE, the degradation pattern for the PE was observed by measuring the Carbonyl Index (CI).[41]

$$\text{Carbonyl Index} = A_1/A_2$$

$A_1$ = peak area of the carbonyl group in FTIR absorption spectrum. $A_2$ = peak area of the CH stretching group in FTIR absorption spectrum.

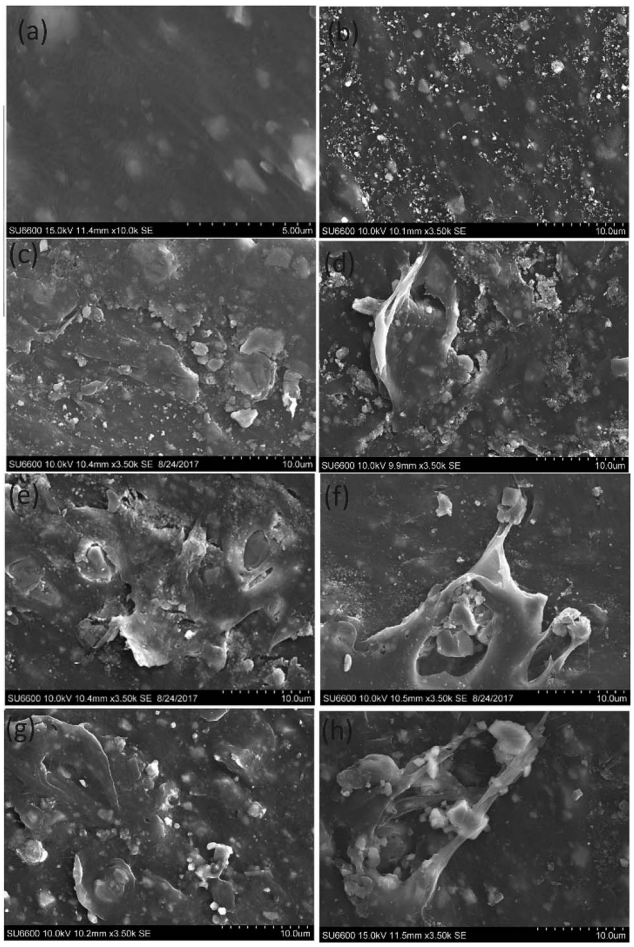


Fig. 6 (a) SEM images of pure PE film, (b–f) SEM images of PE film treated with (b) 5000 ppm, (c) 8000 ppm, (d) 10 000 ppm (e) 11 000 ppm (f) 20 000 ppm of $ZrO_2$ for 20 hours under sun simulator (g and h) SEM images of PE films treated with 10 000 ppm of $TiO_2$ under sun simulator (g) for 20 hours (h) for 100 hours.

For polyethylene

$A_1$ = peak area of the carbonyl group in absorption spectrum (1770–1820 $cm^{-1}$).

$A_2$ = peak area of the CH stretching group in absorption spectrum (2820–2960 $cm^{-1}$).

For polypropylene

$A_1$ = peak area of the carbonyl group in absorption spectrum (1719–1769 $cm^{-1}$).

$A_2$ = peak area of the CH stretching group in absorption spectrum (2744–3004 $cm^{-1}$).

The nanoparticle suspensions with concentrations of 6000, 7000, 8000, 9000, 10 000, 11 000, and 20 000 ppm, respectively, were used to find a concentration which shows sufficient degradation of PE and PP, in order to compare the degradation caused by $TiO_2$ and $ZrO_2$.

All the CI values were calculated using the above formulae and the peak areas were normalized by using the peak area of CH stretching peak

It was observed from Fig. 8, that the CI is increasing when increasing the nanoparticle concentration from 6000 to

 

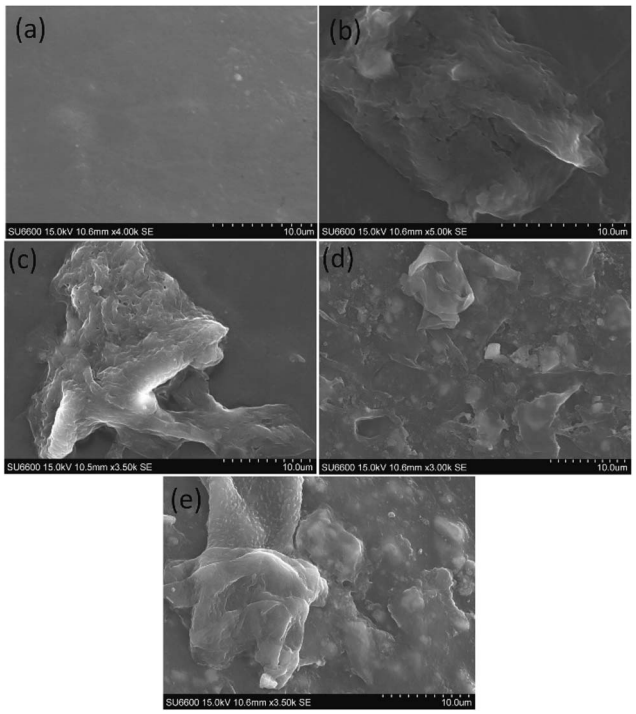


Fig. 7 (a) SEM image of pure PP, (b and c) SEM images of PP films treated with 10 000 ppm (b) $TiO_2$ (c) $ZrO_2$ for 20 hours under real sun light, (d and e) SEM images of PE films treated with 10 000 ppm (d) $TiO_2$ (e) $ZrO_2$ for 20 hours under real sun light.

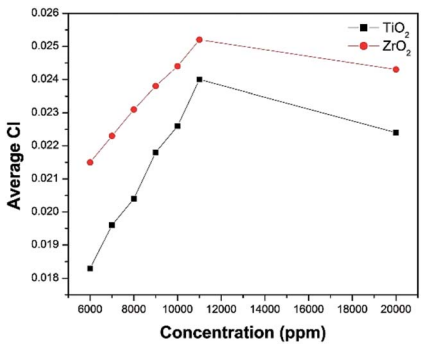


Fig. 8 Average CI *vs.* $TiO_2$ and $ZrO_2$ concentration.

11 000 ppm. When the concentration of $TiO_2$ and $ZrO_2$ increases from 11 000 ppm to 20 000 ppm the carbonyl index decreases. That may be due to the saturation of the PE surface by the nanoparticles. Therefore 10 000 ppm was selected as the nanoparticle concentration for the further studies.

The optimum time required to degrade PE with $TiO_2$ nanoparticles and $ZrO_2$ nanoparticles was determined by replicate measurements at 20, 40, 60, 80, and 100 h, at 10 000 ppm concentration using the sun simulator (Table 1).

The average CI was plotted against the exposure time from 0 to 100 hours (Table 2). When the time is increasing from 0 hours to 20 hours there is a gradual increase in the CI. Within the time range from 20 to 100 hours, there was no significant change in the CI at the 95% confidence level. As there was

Table 1 Averaged CI of PE treated with various $TiO_2$ and $ZrO_2$ concentrations under sun simulator

| Concentration/ppm | Average CI, $TiO_2$ | Average CI, $ZrO_2$ |
|---|---|---|
| 20 000 | 0.0224 | 0.0243 |
| 11 000 | 0.0240 | 0.0252 |
| 10 000 | 0.0226 | 0.0244 |
| 9000 | 0.0218 | 0.0238 |
| 8000 | 0.0204 | 0.0231 |
| 7000 | 0.0196 | 0.0223 |
| 6000 | 0.0183 | 0.0215 |
| 0 | 0.009 | 0.0090 |

Table 2 Average CI of PE treated various times under sun simulator with $TiO_2$

| Time (hours) | Average CI |
|---|---|
| 0 | 0.0091 |
| 20 | 0.0225 |
| 40 | 0.0227 |
| 60 | 0.0230 |
| 80 | 0.0232 |
| 100 | 0.0234 |

a considerable degradation of PE and PP when exposed for 20 hours to the sun simulator 20 hours was selected as the exposure time for the further studies to compare the degradation of $TiO_2$ and $ZrO_2$.

In both treatment conditions (under sun simulator and real sun light) it was found that, at 95% confidence levels, there is a significant difference between the degradation of selected plastics by $ZrO_2$ and $TiO_2$. $ZrO_2$ nanoparticle suspension treated PE and PP samples showed higher degradation than that of the $TiO_2$ treatment (Table 3) (Fig. 9). $TiO_2$ nano particles do not possess a mesoporous characteristic which can result in more efficient light scattering sites inside the mesopore structure.[42] But $ZrO_2$ has a mesoporous structure. That may be one reason for the increased photocatalytic activity of $ZrO_2$ than $TiO_2$. Sreethawong[42] has reported that the mesoporous assembled $ZrO_2$ nano particles showed a comparatively higher degradation of Methyl Orange than commercial P-25 $TiO_2$ nano particles. The presence of oxygen vacancies and their relative abundance in the surface region is considered to be the reason for the

Table 3 Average CI of PE and PP treated under laboratory conditions and the real conditions

| Samples | Polyethylene | | Polypropylene | |
|---|---|---|---|---|
| Treated | Sun simulator | Real conditions | Sun simulator | Real conditions |
| Pure | 0.0090 | 0.0090 | 0.0072 | 0.0072 |
| Untreated | 0.0097 | 0.0175 | 0.0074 | 0.0079 |
| THF | 0.0106 | 0.0183 | 0.0081 | 0.0087 |
| $TiO_2$ | 0.0226 | 0.0260 | 0.0112 | 0.0124 |
| $ZrO_2$ | 0.0244 | 0.0382 | 0.0149 | 0.0190 |

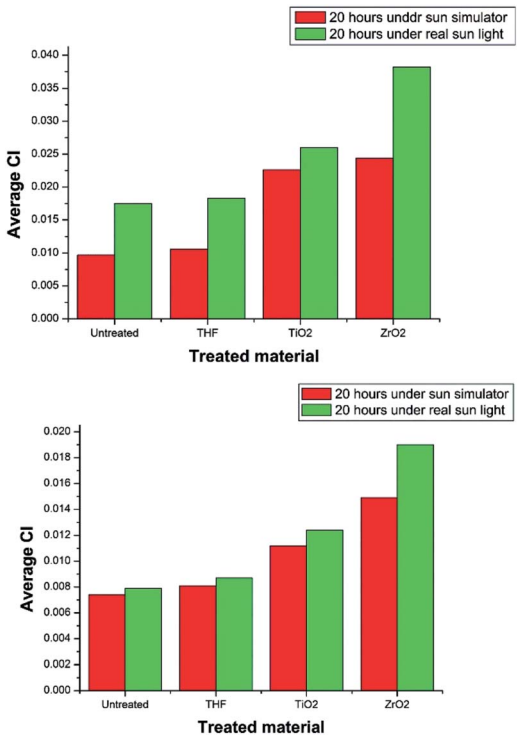


Fig. 9 Average CI variation of (a) PE (b) PP under laboratory conditions and the real conditions.

photocatalytic activity of both $TiO_2$ and $ZrO_2$.[43] $ZrO_2$ has more capability for stabilizing oxygen vacancies than $TiO_2$.[43] Therefore $ZrO_2$ shows more photocatalytic activity than $TiO_2$. It is generally accepted that a higher band gap corresponds to a higher redox ability. According to the UV visible data $ZrO_2$ has a higher band gap energy than $TiO_2$.[44] Thus, due to mesoporous structure, greater capability for stabilizing oxygen vacancies, and the higher band gap, $ZrO_2$ has higher photocatalytic activity than $TiO_2$, and it shows higher degradation of PE and PP than $TiO_2$ under the given experimental conditions.

The degradation of treated PE and PP films in real environmental conditions is superior to that of laboratory conditions. The variation in degradation may result because of the samples were not continuously treated under the direct sun light. They were treated four hours per day and kept in the dark for the rest of the time in order to supply almost a constant intensity of light all the time. When the samples were exposed to the sun light for the first time, the photo catalytic degradation of PE and PP is initiated. As a result, free radicals are formed. That could be the reason for the higher degradation of the PE and PP samples kept under the direct sun light more than the samples kept under the sun simulator. The purpose of treating under the real conditions was to check the eligibility of degradation of PE and PP under direct sun light.

## 4. Conclusion

Successful synthesis of $TiO_2$ and $ZrO_2$ nanoparticles were carried out in this study. $TiO_2$ nanoparticles were tetragonal and they were in the anatase phase. $ZrO_2$ nanoparticles were in the tetragonal phase or a mixture of tetragonal and cubic phases. Concentration optimization and time optimization were done in laboratory conditions under the sun simulator. For both $TiO_2$ and $ZrO_2$ suspensions the optimum concentration was found to be 10 000 ppm, while 20 hours was taken as the optimum time. PE and PP were treated under the sun simulator as well under the real sun light. In both treatment conditions it was found that, with 95% confidence, there is a significant difference between the degradation of selected plastics by $ZrO_2$ and $TiO_2$. $ZrO_2$ nanoparticle suspension treated PE and PP samples showed higher degradation than similar samples treated with the $TiO_2$ nanoparticle suspension. Under these experimental conditions it can be concluded that nano $ZrO_2$ can cause higher photocatalytic degradation than nano $TiO_2$.

## Conflicts of interest

There are no conflicts to declare.

## Acknowledgements

Authors would like to thank Dr Ranil D. Gunarathne for comments that greatly improved the manuscript.

## References

1 A. A. Shah, F. Hasan, A. Hameed and S. Ahmed, *Biotechnol. Adv.*, 2008, **26**, 246–265.
2 H. Webb, J. Arnott, R. Crawford and E. Ivanova, *Polymers*, 2013, **5**, 1.
3 P. Bansal, P. Sharma and V. Goyal, *Biol. Plant.*, 2002, **45**, 125–127.
4 R. Mohee, G. D. Unmar, A. Mudhoo and P. Khadoo, *Waste Manag.*, 2008, **28**, 1624–1629.
5 S. Horikoshi, N. Serpone, Y. Hisamatsu and H. Hidaka, *Environ. Sci. Technol.*, 1998, **32**, 4010–4016.
6 S. K. Kassahun, Z. Kiflie, D. W. Shin, S. S. Park, W. Y. Jung and Y. R. Chung, *J. Sol-Gel Sci. Technol.*, 2017, **82**, 322–334.
7 J. Zhang, P. Zhou, J. Liu and J. Yu, *Phys. Chem. Chem. Phys.*, 2014, **16**, 20382–20386.
8 M. N. Chong, B. Jin, C. W. Chow and C. Saint, *Water Res.*, 2010, **44**, 2997–3027.
9 B. Neppolian, S. Mine, Y. Horiuchi, C. Bianchi, M. Matsuoka, D. Dionysiou and M. Anpo, *Chemosphere*, 2016, **153**, 237–243.
10 M. Dissanayake, H. Divarathna, C. Dissanayake, G. Senadeera, P. Ekanayake and C. Thotawattage, *J. Photochem. Photobiol., A*, 2016, **322**, 110–118.
11 I. Junkar, M. Kulkarni, B. Drašler, N. Rugelj, A. Mazare, A. Flašker, D. Drobne, P. Humpolíček, M. Resnik and P. Schmuki, *Bioelectrochemistry*, 2016, **109**, 79–86.
12 K. Gulati, L. Johnson, R. Karunagaran, D. Findlay and D. Losic, *Biomacromolecules*, 2016, **17**, 1261–1271.
13 R. N. Wijesena, N. D. Tissera, R. Perera, K. N. de Silva and G. A. Amaratunga, *J. Mol. Catal. A: Chem.*, 2015, **398**, 107–114.
14 A. Kadam, R. Dhabbe, M. Kokate, Y. Gaikwad and K. Garadkar, *Spectrochim. Acta, Part A*, 2014, **133**, 669–676.

 

15 X.-H. Ning, Q.-L. Meng, Y.-L. Han, D.-Y. Zhou, L. Li, L. Cao, Z.-K. Weng, R. Ding and Z.-B. Wang, *RSC Adv.*, 2017, **7**, 34907–34911.
16 A. Singhania and S. M. Gupta, *Beilstein J. Nanotechnol.*, 2017, **8**, 264.
17 J. A. Navío, M. C. Hidalgo, G. Colón, S. G. Botta and M. I. Litter, *Langmuir*, 2001, **17**, 202–210.
18 G.-L. Tan and X.-J. Wu, *Thin Solid Films*, 1998, **330**, 59–61.
19 Y. Chu, Y. Chen, N. Chen, F. Wang and H. Zhu, *RSC Adv.*, 2016, **6**, 96768–96777.
20 Z. Guerra-Que, G. Torres-Torres, H. Perez-Vidal, I. Cuauhtemoc-Lopez, A. Espinosa de los Monteros, J. N. Beltramini and D. M. Frias-Marquez, *RSC Adv.*, 2017, **7**, 3599–3610.
21 S.-y. Li, Y. Wang, J.-G. Wu, L.-f. Guo, M. Ye, Y.-H. Shao, R. Wang, C.-e. Zhao and A. Wei, *RSC Adv.*, 2016, **6**, 72037–72043.
22 T. A. Maia and E. M. Assaf, *RSC Adv.*, 2014, **4**, 31142–31154.
23 M. Tamura, T. Kitanaka, Y. Nakagawa and K. Tomishige, *ACS Catal.*, 2016, **6**, 376–380.
24 T. A. Cheema and G. Garnweitner, *CrystEngComm*, 2014, **16**, 3366–3375.
25 M. Ranjbar, M. Yousefi, M. Lahooti and A. Malekzadeh, *Int. J. Biomed. Nanosci. Nanotechnol.*, 2012, **8**, 191–196.
26 L. Zhou, A. Zhao, Z. Wang, Z. Chen, J. Ren and X. Qu, *ACS Appl. Mater. Interfaces*, 2015, **7**, 2905–2911.
27 C. Khatua, I. Chinya, D. Saha, S. Das, R. Sen and A. Dhara, *Int. J. Smart Sens. Intell. Syst.*, 2015, **8**, 1424–1442.
28 S. Mugundan, B. Rajamannan, G. Viruthagiri, N. Shanmugam, R. Gobi and P. Praveen, *Appl. Nanosci.*, 2015, **5**, 449–456.
29 K. Anandan and V. Rajendran, *J. Phys. Sci.*, 2013, **17**, 179–184.
30 S. Jayakumar, P. Ananthapadmanabhan, T. Thiyagarajan, K. Perumal, S. Mishra, G. Suresh, L. Su and A. Tok, *Mater. Chem. Phys.*, 2013, **140**, 176–182.
31 Y. Yu, X. Wang, Y. Cao and X. Hu, *Appl. Surf. Sci.*, 2001, **172**, 260–264.
32 J. M. Pettibone, D. M. Cwiertny, M. Scherer and V. H. Grassian, *Langmuir*, 2008, **24**, 6659–6667.
33 S. N. Basahel, T. T. Ali, M. Mokhtar and K. Narasimharao, *Nanoscale Res. Lett.*, 2015, **10**, 73.
34 X. Meng, D.-W. Shin, S. M. Yu, J. H. Jung, H. I. Kim, H. M. Lee, Y.-H. Han, V. Bhoraskar and J.-B. Yoo, *CrystEngComm*, 2011, **13**, 3021–3029.
35 C. Dette, M. A. Pérez-Osorio, C. S. Kley, P. Punke, C. E. Patrick, P. Jacobson, F. Giustino, S. J. Jung and K. Kern, *Nano Lett.*, 2014, **14**, 6533–6538.
36 J.-P. Xu, R.-J. Zhang, Y. Zhang, Z.-Y. Wang, L. Chen, Q.-H. Huang, H.-L. Lu, S.-Y. Wang, Y.-X. Zheng and L.-Y. Chen, *Phys. Chem. Chem. Phys.*, 2016, **18**, 3316–3321.
37 S. Liu, W. Wang, J. Chen, J.-G. Li, X. Li, X. Sun and Y. Dong, *J. Mater. Chem. A*, 2015, **3**, 17837–17848.
38 H. M. Moghaddam and S. Nasirian, *S. Afr. J. Sci.*, 2011, **107**, 01–05.
39 A. L. Forster, A. M. Forster, J. W. Chin, J.-S. Peng, C.-C. Lin, S. Petit, K.-L. Kang, N. Paulter, M. A. Riley and K. D. Rice, *Polym. Degrad. Stab.*, 2015, **114**, 45–51.
40 D. J. Nagle, G. A. George, L. Rintoul and P. M. Fredericks, *Vib. Spectrosc.*, 2010, **53**, 24–27.
41 A. Eshraghi, H. Khademieslam, I. Ghasemi and M. Talaiepoor, *BioResources*, 2012, **8**, 201–210.
42 T. Sreethawong, S. Ngamsinlapasathian and S. Yoshikawa, *Chem. Eng. J.*, 2013, **228**, 256–262.
43 S. Tosoni, H. Y. T. Chen and G. Pacchioni, *ChemPhysChem*, 2015, **16**, 3642–3651.
44 B. M. Pirzada, N. A. Mir, N. Qutub, O. Mehraj, S. Sabir and M. Muneer, *Mater. Sci. Eng., B*, 2015, **193**, 137–145.